Medium Thickness Estimation Technique Based on Angular-Frequency Correlation Function

Sermsak Jaruwatanadilok, Rasmus Solmer Eriksen, and Yasuo Kuga

***Abstract*—This paper discusses a new method to estimate the medium thickness based on the angular-frequency correlation function (ACF/FCF). The angular-frequency correlation function has been shown to suppress the clutter in radar imaging applications. Under real-world scenarios with rough surfaces and particle inclusions, it has unique characteristics, namely, memory line and memory dots, which can be useful for extracting medium characteristics. We derive the analytical solution for the ACF/FCF of a multi-layer medium model using the ACBD matrix and first-order Kirchhoff approximation. We also conduct experiments to verify the method. We show that the phase information of the ACF/FCF can be used to retrieve the thickness information of the medium. This method has potential applications in the remote sensing of sea-ice and snow.**

***Index Terms*—Scattering, Remote sensing, Snow, Sea ice**

I. Introduction

THE abiliy to retrieve the parameters of sea-ice and snow using remotely sensed data is crucial to wide-scale earth monitoring, especially in relation to the state of the climate and global warming phenomena. Electromagnetic waves, either from an aircraft or satellite, have been used extensively in this application by imaging and sensing using the radar cross section. Satellite images are used to estimate the extent of the ice cover in the North Pole, South Pole and Greenland. Several works have been devoted to the estimation of parameters of sea-ice and snow [1-9]. One of the most important parameters is the sea-ice and snow depth. The thickness of sea-ice can be used to estimate the sea-ice volume which indicates the hydrological and climate state of the environment. The snow depth is also very important, especially, the snow-cover on land because it is the indication of water equivalent that determines the water run-off after the snow melts.

In this paper, we explain a new retrieval method based on the angular-frequency correlation function. The central idea is to employ active remote sensing by sending two waves at different frequencies and angles and use the backscattering signals to form correlation functions. Because this wave correlation is for waves with two different frequencies and incident angles, we call it 'angular-frequency correlation function' (ACF/FCF). ACF/FCF has been used previously in the retrieval of the roughness characteristics of the surface [10], and object detection and imaging under a rough surface [11,12]. We derive the formulation of this ACF/FCF of a multi-layer mediun with rough surface interfaces using the ABCD matrix method and the first-order Kirchhoff approximation. This correlation function exhibits a unique feature called 'memory line', which is a line of strong correlation when incident angles and observation angles vary. Using this memory line, we are able to choose the optimum combination of frequencies and angles to get a measurement for ACF/FCF. The phase of ACF/FCF shows relationship with the medium thickness and its dielectric constant. Thus, we employ the phase of ACF/FCF to retrieve the medium thickness. We performed experiments to verify the existence of the memory line and showed that the forward model of the two-dimensional rough surface coincides with the experimental data. We also show the effectiveness of the medium thickness retrieval based on ACF/FCF information.

This work was supported in part by the Jet Propulsion Laboratory

S. Jaruwatanadilok and Y. Kuga are with the Electrical Engineering Department, University of Washington, Seattle, WA, 98195 USA, (e-mail: sermsak@ee.washington.edu).

R. S. Eriksen is with Technical University of Denmark.

II. Theory – ACF/FCF for multi-layer media

A. Multi-layer media model – coherent component

The multi-layer media model used in this work consists of four layers with rough surface interfaces as shown in Fig. 1.

First, we consider the coherent component as shown in Fig. 2. Using the ABCD matrix method [13], we can calculate the up-going and down-going waves as

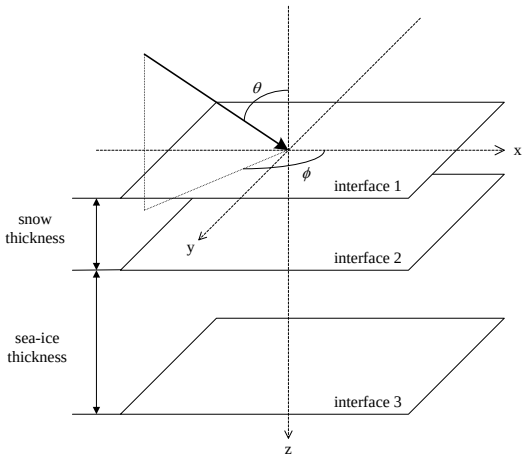

Fig. 1. Multi-layer model

$$\begin{bmatrix}\psi_{d1}\\ \psi_{u1}\end{bmatrix}=\begin{bmatrix}E_o\\ R_s E_o\end{bmatrix}, \tag{1}$$

$$\psi_{d2}=E_o\exp(jq_2h_2)\left\{\left(\left(1+R_s\right)+\frac{(1-R_s)}{Z_1}\right)\cos q_2h_2 + j\left(\frac{(1-R_s)Z_2}{Z_1}+\frac{(1+R_s)}{Z_2}\right)\sin q_2h_2\right\},$$

$$\psi_{u2}=E_o\exp(-jq_2h_2)\left\{\left(\left(1+R_s\right)-\frac{(1-R_s)}{Z_1}\right)\cos q_2h_2 + j\left(\frac{(1-R_s)Z_2}{Z_1}-\frac{(1+R_s)}{Z_2}\right)\sin q_2h_2\right\}, \tag{2}$$

and

$$\begin{bmatrix}\psi_{d3}\\ \psi_{u3}\end{bmatrix}=\begin{bmatrix}\left(\frac{E_oT_s}{2}\left(1+\frac{Z_3}{Z_4}\right)\right)\exp(jq_3h_3)\\ \left(\frac{E_oT_s}{2}\left(1-\frac{Z_3}{Z_4}\right)\right)\exp(-jq_3h_3)\end{bmatrix} \tag{3}$$

where $R_s=\dfrac{A+B/Z_4-Z_1(C+D/Z_4)}{A+B/Z_4+Z_1(C+D/Z_4)}$,

$T_s=\dfrac{2}{A+B/Z_4+Z_1(C+D/Z_4)}$,

$\begin{bmatrix}A & B\\ C & D\end{bmatrix}=\begin{bmatrix}A_2 & B_2\\ C_2 & D_2\end{bmatrix}\begin{bmatrix}A_3 & B_3\\ C_3 & D_3\end{bmatrix}$,

$A_m=D_m=\cos q_mh_m$, $B_m=jZ_m\sin q_mh_m$, $C_m=\dfrac{j\sin q_mh_m}{Z_m}$,

$q_m=\beta_m\cos(\theta_m)-j\alpha_m$. For perpendicular polarization (TE) wave, $Z_m=\dfrac{\omega\mu_m}{q_m}$ and for parallel polarization (TM) wave, $Z_m=\dfrac{q_m}{\omega\mu_m}$. These up-going and down-going waves are used in the calculation of the correlation function when the incoherent component is considered.

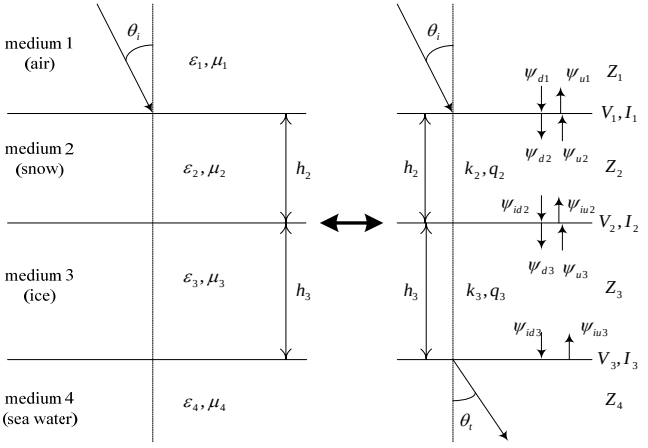

Fig. 2. ABCD matrix model

B. *Incoherent component – Kirchhoff approximation*

The coherent components are the scattering from the rough surfaces. Considering the rough surface as shown in Fig. 3, we apply the Kirchhoff approximation to calculate the correlation of waves from rough surface scattering. The correlation formulation is given by [14]

$$\Gamma=\frac{\exp(-jkR)}{R}\frac{\exp(jk'R)}{R}\left\langle\bar{F}(\omega,\theta)\bar{F}^*(\omega',\theta')\right\rangle \tag{4}$$

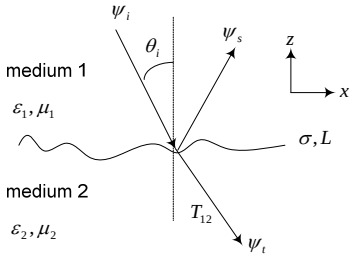

Fig. 3. Rough surface geometry

We only consider the first-order case where, for the TM case, we get

$$\Gamma=\frac{\exp\left(-j(k-k')R\right)}{R^2}\left\langle f_{11}(\omega,\theta)\,f_{11}^*(\omega',\theta')\right\rangle \tag{5}$$

where $\left\langle f_{11}(\omega,\theta)\,f_{11}^*(\omega',\theta')\right\rangle=H_{11}(\omega,\theta)H_{11}^*(\omega',\theta')I^{(1)}$. For the TE case, we get

$$\Gamma=\frac{\exp\left(-j(k-k')R\right)}{R^2}\left\langle f_{22}(\omega,\theta)\,f_{22}^*(\omega',\theta')\right\rangle \tag{6}$$

where $\left\langle f_{22}(\omega,\theta)\,f_{22}^*(\omega',\theta')\right\rangle=H_{22}(\omega,\theta)H_{22}^*(\omega',\theta')I^{(1)}$, and $I^{(1)}=\left\langle J_1(\omega,\theta)J_1^*(\omega',\theta')\right\rangle-\left\langle J_1(\omega,\theta)\right\rangle\left\langle J_1^*(\omega',\theta')\right\rangle$. We assume that $I^{(1)}=\left\langle J_1(\omega,\theta)J_1^*(\omega',\theta')\right\rangle$, from [14], we get

$$\left\langle J_1(\omega,\theta)J_1^*(\omega',\theta')\right\rangle=\Phi_1\Phi_{s1}S(\theta_i,\theta_o)S(\theta_i',\theta_o') \tag{7}$$

where $\Phi_1=\dfrac{\exp\left(-\frac{\sigma^2}{2}(v_z-v_z')^2\right)}{N_zN_z'}\left(\dfrac{\pi L^2}{v_zv_z'\sigma^2}\right)\exp\left(-\dfrac{|\bar{v}_c|^2L^2}{4v_zv_z'\sigma^2}\right)$,

$\Phi_{s1}=\left(\pi L_{xeq}L_{yeq}\right)\exp\left(-\dfrac{v_{dx}^2L_{xeq}^2}{4}-\dfrac{v_{dy}^2L_{yeq}^2}{4}\right)$, $\bar{K}-\bar{K}_i=\bar{v}+v_z\hat{z}$,

$\bar{K}'-\bar{K}_i'=\bar{v}'+v_z'\hat{z}$, $\bar{v}_c=\dfrac{1}{2}(\bar{v}+\bar{v}')$, $\bar{v}_d=(\bar{v}-\bar{v}')$,

$N_z=\dfrac{v_z}{|\bar{K}-\bar{K}_i|}$, $N_z'=\dfrac{v_z'}{|\bar{K}'-\bar{K}_i'|}$, L is the correlation length, σ is the rms height, L_{xeq} is the illumination length in *x*-direction, and L_{yeq} is the illumination length in *y*-direction. The function H_{11} and H_{22} is given by

$$[H]=\begin{bmatrix}H_{11} & H_{12}\\ H_{21} & H_{22}\end{bmatrix}=\frac{1}{4\pi}\left(j[\hat{K}][\hat{K}][\hat{n}_1][\hat{r}]\frac{1}{k}+[\hat{K}][\hat{n}_1]\right)[e_{1s}]$$

where $[e_{1s}] = R_{\parallel}[p_r][p]^{\dagger} + R_{\perp}[q][q]^{\dagger}$, $[q] = \dfrac{[\hat{i}][n_1]}{\sqrt{1-\left([\hat{i}][n_1]\right)^2}}$,

$[p] = [\hat{q}][i]$, $[p_r] = [\hat{r}][q]$, $[\hat{r}] = [i] - 2[n_1]\left([n_1]^{\dagger}[i]\right)$,

$[n_1] = \dfrac{[o]-[i]}{\sqrt{([o]-[i])^{\dagger}([o]-[i])}}$, $K = k\hat{o}$, $K_i = k\hat{i}$,

$$[o] = \begin{bmatrix} \sin\theta\cos\phi \\ \sin\theta\sin\phi \\ \cos\theta \end{bmatrix},\ [i] = \begin{bmatrix} \sin\theta_i \\ 0 \\ -\cos\theta_i \end{bmatrix},\ [\theta] = \begin{bmatrix} \cos\theta\cos\phi \\ \cos\theta\sin\phi \\ -\sin\theta \end{bmatrix},$$

$$[\theta_i] = \begin{bmatrix} -\cos\theta_i \\ 0 \\ -\sin\theta_i \end{bmatrix},\ [\phi] = \begin{bmatrix} -\sin\phi \\ \cos\phi \\ 0 \end{bmatrix},\ [\phi_i] = \begin{bmatrix} 0 \\ 1 \\ 0 \end{bmatrix},$$

$$R_{\parallel} = \frac{\sqrt{\varepsilon_1}\cos\theta_2 - \sqrt{\varepsilon_2}\cos\theta_1}{\sqrt{\varepsilon_1}\cos\theta_2 + \sqrt{\varepsilon_2}\cos\theta_1},\ R_{\perp} = \frac{\sqrt{\varepsilon_1}\cos\theta_1 - \sqrt{\varepsilon_2}\cos\theta_2}{\sqrt{\varepsilon_1}\cos\theta_1 + \sqrt{\varepsilon_2}\cos\theta_2}.$$

We also define $[\hat{B}][C] = \begin{bmatrix} 0 & -B_z & B_y \\ B_z & 0 & -B_x \\ -B_y & B_x & 0 \end{bmatrix}\begin{bmatrix} C_x \\ C_y \\ C_z \end{bmatrix}$.

III. Numerical Calculations and Experimental Results

A. Experimental setup

We performed experiments in the Ka band (30-40 GHz) with the setup schematic in Fig. 4. An Agilent 8722ET vector network analyzer was used to measure the backscattered waves. The rough surface is placed on a turntable that can be computer-controlled to rotate. The antenna is mounted on a boom above the surface, at a distance in the order of the antenna far field distance, and the boom is mounted on a rotational stage that rotates around the horizontal axis. Both axis drives are driven by stepping motors which eliminate the need for electronic position feedback. The photo of the experimental set up is shown in Fig. 5.

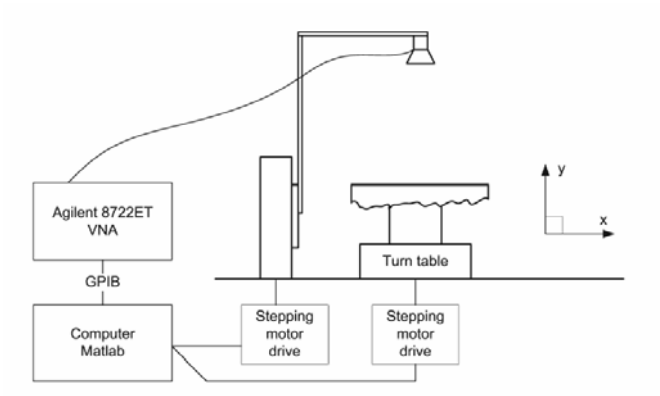

Fig. 4. Schematic of the experimental setup

The medium used in the experiment is a slab of low-density dielectric with a smooth surface on one side and a rough surface with conducting graphite paint on the other side. The rough surface has a Gaussian characteristic with the rms height (σ) of 3 mm and correlation length (L) of 12 mm. A side cut of the medium is shown schematically in Fig. 6.

Fig. 5. Photo of the experimental setup

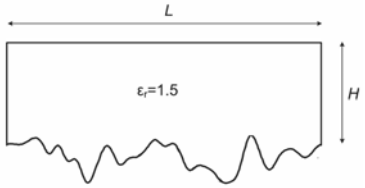

Fig. 6. A side cut of the medium ('thin'). L = 30 cm and H = 3 cm.

We performed experiments by, first, fixing the incident angle at 19°, and then varying the frequency from 30 GHz to 40 GHz with the step of 250 MHz creating 401 data points. Then, we rotate the turntable by 20° and repeat the process. This rotation of the turntable is to create other scattering events for an ensemble average process in the correlation function calculation. Next, we perform the same measurement when the incident angle is fixed at 20°. The backscattered waves at 19° incident and 20° incident in the same configuration are then correlated using

$$\mathbf{C} = \frac{1}{N}\sum_{i=1}^{N}\left[\mathbf{L}_1^H(i)\mathbf{L}_2(i)\right]^T \qquad (8)$$

where $\mathbf{C}$ is 401 by 401 correlation matrix. The vector $\mathbf{L}_1$ is the 1 by 401 vector from the measurement at incident angle of 19°, and the vector $\mathbf{L}_2$ is the 1 by 401 vector from the measurement at incident angle of 20°. The iteration i indicates the 'ensemble', which is the position of the rotated rough surface, and H denotes the conjugate transpose. Based on our data analysis, we use $N = 20$.

B. Comparison of analytical and experimental results

We apply the analytical solution explained in the previous section with some modifications. The modifications of the analytical solution are assumptions that the characteristics of medium 2 are set to equal to those of medium 1, which effectively reduce the problem to a three-layer medium. Also, for the last medium, we put in the characteristics of a conducting material. Thus, the modified analytical solution

represents the experimental setup. We compute the correlation function by fixing incident and observation angles and varying the frequency as described previously in the experiment setup. The results are pictures of the 'memory line'. We compare the memory lines obtained by analytical solution with those obtained from the experiments, and the results are shown in Fig. 7.

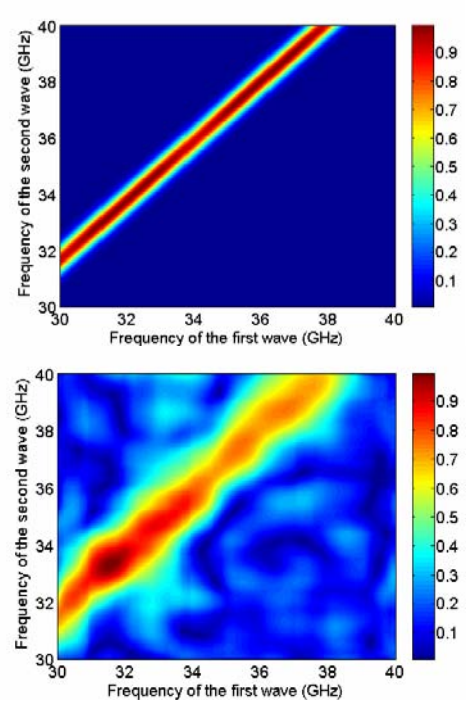

Fig. 7. Memory line phenomenon. Top: Analytical solution, Bottom: Experimental data

The results verify the existence of the memory line phenomenon on the expected angle and frequency combinations. This strong correlation enables the retrieval of the wave correlation information. Because we will use phase information for thickness retrieval, the phase information verification is crucial. The comparison of the phase of the correlation function from the analytical solution and the experimental data is shown in Fig. 8.

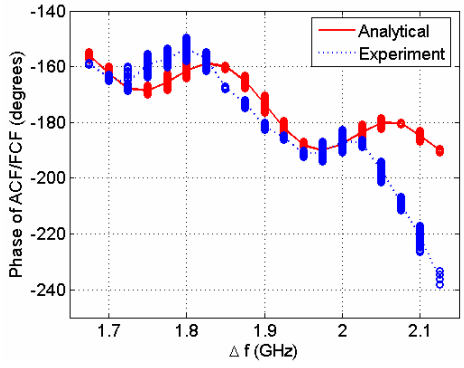

Fig. 8. Comparison of phase of the correlation function

We further investigate the effect of the thickness of the medium to the correlation function. In the experiments, we put a slab of the same medium on top of another medium as shown in Fig. 9. Then, we investigated the memory line and the result is shown in Fig. 10. Compared to the memory line in the 'thin' case in Fig. 7, the memory line in the 'thick' case locates in the same combination of angles and frequencies. However, the memory line appears to be thicker. Now, we compare the phase characteristics of the correlation function in the 'thick' and 'thin' cases. The results are illustrated in Fig. 11.

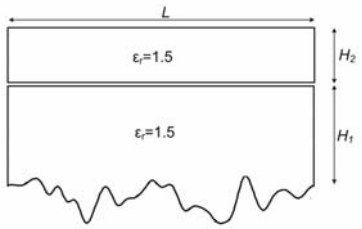

Fig. 9. A side cut of the second configuration medium ('thick'). L = 30 cm and H_1 = 3 cm, H_2 = 1.6 cm.

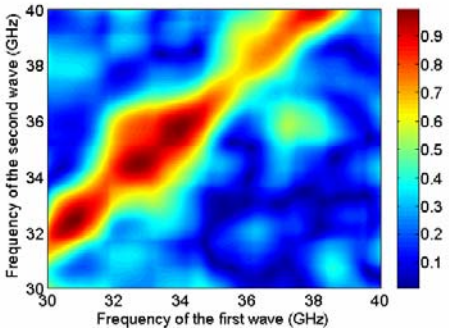

Fig. 10. Memory line from experimental data in the 'thick' case

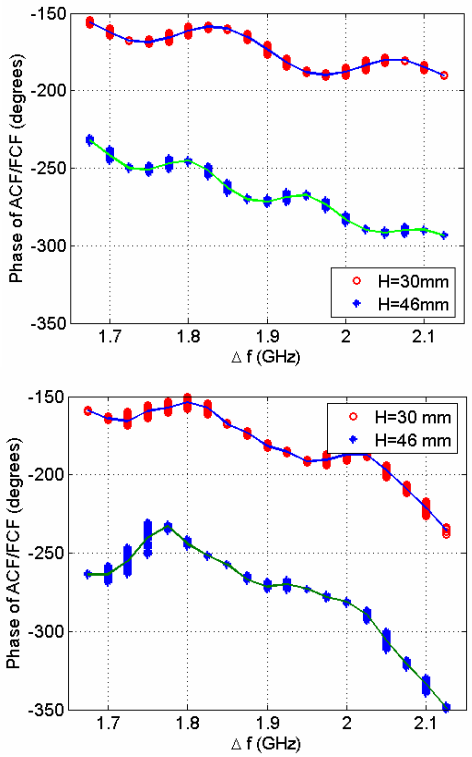

Fig. 11. Comparison of phase of the correlation function. Top: Analytical solution, Bottom: Experimental data

C. *Inversion method for medium thickness retrieval*

We use the phase from the frequency difference to determine the thickness. The estimated thickness is approximately

$$h_{est} = \frac{c|\phi|\cos\theta}{4\pi\Delta f} \tag{9}$$

where c is the speed of light in the medium $= 3\times10^8/\sqrt{\varepsilon_r}$, θ is the incident angle, Δf is the frequency difference, and ϕ is the phase of the ACF/FCF. This formula is valid for the case where the incident angles of the two waves are very close. In our case, the incident angles are 19° and 20°. From this formula, we can estimate the thickness of the medium using the phase information shown in Fig. 11. The results, which are illustrated in Fig. 12, show variations as a function of the frequency difference. However, when we average these estimations, we get an estimate of 30.4 mm and 46.4 mm for the experimental data and 29.3 mm and 44.9 mm for the analytical solution in the case of 'thin' and 'thick,

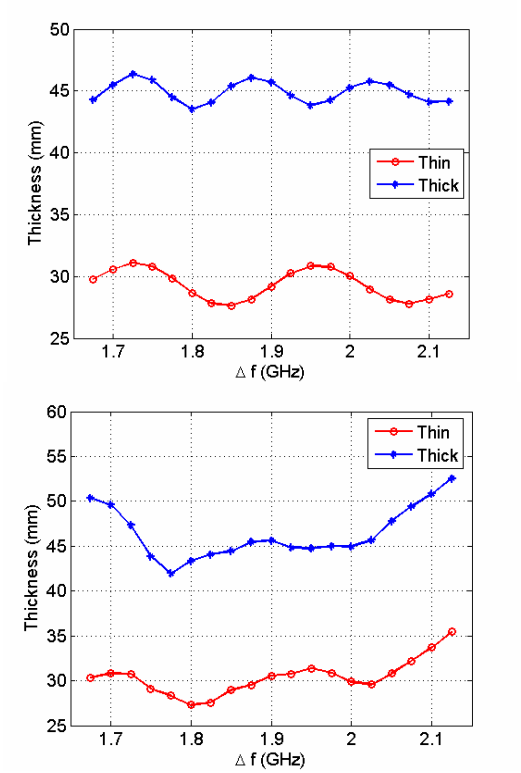

Fig. 12. Estimation of the medium thickness. Top: Analytical solution, Bottom: Experimental data

respectively.

IV. Conclusions

We present a new method to estimate the thickness of the medium based on angular-frequency correlation function. The phase of the ACF/FCF is used to retrieve the thickness of the medium. We present the analytical solution of a multi-layer rough surface model based on the ABCD matrix and Kirchhoff approximation. Experiments are performed to verify the analytical solution and the retrieval method. Good agreement is observed in the comparison of experiments and the analytical solution. We also show that this new method can effectively retrieve the thickness of the medium with good accuracy.

Acknowledgment

This work is supported by the Jet Propulsion Laboratory.

References

[1] S. Jaruwatanadilok, A. Ishimaru, and Y. Kuga, "Snow thickness estimation using correlation function," *IGARSS 2004*, Anchorage, Alaska, September 20-24, 2004.

[2] Z. A. Hussein, Y. Kuga, A. Ishimaru, S. Jaruwatanadilok, and K. Pak, "Angular and frequency correlation for sea-ice thickness retrieval," *IGARSS 2004*, Anchorage, Alaska, September 20-24, 2004.

[3] P. Wadhams, M. A. Lange, and S. F. Ackley, "The ice thickness distribution across the Atlantic sector of the Antarctic Ocean in midwinter," *Journal of Geophysical Research*, vol. 92, pp. 14535-52, 1987.

[4] D. T. Davis, Z. X. Chen, J. N. Hwang, A. T. C. Chang, and L. Tsang, "Retrieval of Snow Parameters by Iterative Inversion of a Neural-Network," *IEEE Transactions on Geoscience and Remote Sensing*, vol. 31, pp. 842-852, 1993.

[5] A. Kovacs and J. S. Holladay, "Sea-ice thickness measurement using a small airborne electromagnetic sounding system," *Geophysics*, vol. 55, pp. 1327-37, 1990.

[6] G. T. Lei, R. K. Moore, and S. Gogineni, "A Method for Measuring Snow Depth Using Fine-Resolution Radars," *Remote Sensing of Environment*, vol. 30, pp. 151-158, 1989.

[7] Y. Bo and X. Feng, "The retrieval of snow-depth using SSM/I remotely sensed data and its results assessment in Qinghai-Xizang (Tibet) plateau," IEEE International Geoscience and Remote Sensing Symposium, Honolulu, HI, USA, 24-28 July 2000.

[8] F. Papa, B. Legresy, N. M. Mognard, E. G. Josberger, and F. Remy, "Estimating terrestrial snow depth with the Topex-Poseidon altimeter and radiometer," *IEEE Transactions on Geoscience and Remote Sensing*, vol. 40, pp. 2162-2169, 2002.

[9] J. R. Wang, A. T. C. Chang, and A. K. Sharma, "On the Estimation of Snow Depth from Microwave Radiometric Measurements," *IEEE Transactions on Geoscience and Remote Sensing*, vol. 30, pp. 785-792, 1992.

[10] C. T. C. Le, A. Ishimaru, Y. Kuga, and J. H. Yea, "Angular memory and frequency interferometry for mean height profiling of a rough surface," *IEEE Transactions on Geoscience and Remote Sensing*, vol. 36, pp. 61-71, 1998.

[11] G. F. Zhang and L. Tsang, "Angular correlation function of wave scattering by a random rough surface and discrete scatterers and its application in the detection of a buried object," *Waves in Random Media*, vol. 7, pp. 467-478, 1997.

[12] G. Zhang and L. Tsang, "Application of angular correlation function of clutter scattering and correlation imaging in target detection," *IEEE Transactions on Geoscience and Remote Sensing*, vol. 36, pp. 1485-93, 1998.

[13] A. Ishimaru, *Wave Propagation and Scattering in Random Media*, IEEE Press, Piscataway, New Jersey and Oxford University Press, Oxford, England, An IEEE-OUP Classic Reissue, 1997.

[14] A. Ishimaru, C. T. C. Le, Y. Kuga, L. Ailes-Sengers, and T.-K. Chan, "Polarimetric scattering theory for high slope rough surfaces," *Journal of Electromagnetic Waves and Applications*, vol. 10, no. 4, pp. 489-491, 1996.